Sliding dynamics for bubble phases on periodic modulated substrates

C. Reichhardt and C. J. O. Reichhardt
Theoretical Division and Center for Nonlinear Studies, Los Alamos National Laboratory, Los Alamos, New Mexico 87545, USA

(Received 24 January 2024; accepted 19 April 2024; published 2 May 2024)

We analyze a bubble-forming system composed of particles with competing long-range repulsive and short-range attractive interactions driven over a quasi-one-dimensional periodic substrate. We find various pinned and sliding phases as a function of substrate strength and drive amplitude. When the substrate is weak, a pinned bubble phase appears that depins elastically into a sliding bubble lattice. For stronger substrates, we find anisotropic bubbles, disordered bubbles, and stripe phases. Plastic depinning occurs via the hopping of individual particles from one bubble to the next in a pinned bubble lattice, and as the drive increases, there is a transition to a state where all of the bubbles are moving but are continuously shedding and absorbing individual particles. This is followed at high drives by a moving bubble lattice in which the particles can no longer escape their individual bubbles. The transition between the plastic and elastic sliding phases can be detected via signatures in the velocity-force curves, differential conductivity, and noise. When the bubbles shrink due to an increase in the attractive interaction term, they fit better inside the pinning troughs and become more strongly pinned, leading to a reentrant pinning phase. For weaker attractive terms, the size of the bubbles becomes greater than the width of the pinning troughs and the depinning becomes elastic with a reduced depinning threshold.

DOI: 10.1103/PhysRevResearch.6.023116

I. INTRODUCTION

There are a variety of particle systems that can form bubble phases exhibiting two length scales, with the shorter scale determined by the average spacing between particles that are confined inside an individual bubble, and the larger scale arising from the assembly of the bubbles themselves into an ordered lattice. Bubble lattices typically appear when there is a competition between attractive and repulsive interactions, such as short-range attraction and longer-range repulsion [1–9]. The bubbles can distort and break up into smaller bubbles as a function of temperature or as a result of interacting with quenched disorder [2]. Bubble phases known as mesophases arise in colloidal systems that have multiple length scales, such as multistep repulsive interactions [10–13]. Bubble phases can also appear in superconducting systems for vortices with competing interactions [14–20], as well as for magnetic skyrmion-superconducting vortex hybrids [21]. Bubbles containing two or more particles can form when charge ordering occurs in two-dimensional election systems [22–27]. In a system with competing interactions, the bubbles are often only one of several types of possible phases, including crystals, stripes, and void lattices, that arise as a function of particle density or the ratio of the repulsive and attractive interaction terms [7,11,13,28–30]. The bubble phases occur for lower densities or stronger attractive interaction terms. There are also a variety of bubblelike systems where the bubble textures can distort or the shape can change, including emulsions and magnetic textures such as skyrmions [31].

Bubble lattices can interact with a substrate, which for soft matter systems could be created using optical trap arrays [32–37] or patterned surfaces [38]. In solid-state systems, ordered substrates can be made using various nanostructuring techniques. One of the simplest substrate geometries is a periodic quasi-one-dimensional (q1D) arrangement of troughs, which can induce the formation of various crystalline, smectic, and disordered phases for purely repulsive colloidal particles as a function of the trough strength and the ratio of the number of particles to the number of troughs [39–46]. Different kinds of vortex patterns and depinning phenomena have been studied in superconducting systems for vortices interacting with periodic q1D substrates [47–49]. Far less is known about what happens when bubble- or pattern-forming systems with competing interactions are coupled to a periodic substrate, and the depinning or sliding dynamics under a drive have received even less study. McDermott *et al.* [50] considered a pattern-forming system with competing repulsion and attraction on periodic q1D substrates, and found that for a parameter regime where the system forms a stripe phase in the absence of the substrate, several stripe and modulated stripe phases as well as kinks appear as a function of substrate strength or substrate lattice spacing.

Here, we examine the statics and dynamics of particles with competing long-range repulsion and short-range attraction interacting with a periodic q1D substrate in the limit where the system forms a bubble phase in the absence of a substrate. For weak substrates, a triangular bubble lattice appears that becomes increasingly anisotropic as the substrate strength increases. When an external drive is applied to the system, the depinning transition can be elastic, where each bubble retains its original set of particles, or plastic, where the bubble lattice remains pinned but individual particles hop from one bubble to the next. At higher drives, a bubble-shedding phase can appear in which all of the bubbles are moving but a portion of the particles can break away from one moving bubble and become attached to a different moving bubble, while a dynamic reordering transition into a moving elastic bubble lattice occurs for sufficiently large driving forces. In the plastic flow regime, we find a phase that we term a sliding bubble track phase, in which stripes of particles remain pinned to the substrate and form tracks along which the bubbles travel. We show that the nature of the depinning transition and the net velocity depend strongly on whether an individual bubble can fit into a single substrate trough, and demonstrate that smaller bubbles are more easily pinned. This leads to the emergence of reentrant pinning as a function of bubble size, where for constant applied drive the bubbles repin as they become smaller. Bubbles that are larger than the width of the substrate troughs can slide easily in an elastic phase. Our results should be relevant to a variety of bubble-forming systems on q1D substrates, including electron bubbles, colloidal particles, and magnetic skyrmions.

II. SIMULATION

We examine a two-dimensional (2D) system of N particles whose pairwise interactions have a long-range repulsive term and a short-range attractive term. The sample is of size $L \times L$ with $L = 36$ and has periodic boundary conditions in the x and y directions. The particle density is $\rho = N/L^2$. The particles interact with a periodic q1D substrate and are subjected to a dc driving force. The following overdamped equation governs the dynamics of particle i:

$$\eta \frac{d\mathbf{R}_i}{dt} = -\sum_{j\neq i}^{N} \nabla V(R_{ij}) + \mathbf{F}_i^s + \mathbf{F}_D, \quad (1)$$

where the damping term η is set to $\eta = 1.0$.

The particle-particle interaction potential is given by

$$V(R_{ij}) = \frac{1}{R_{ij}} - B\exp(-\kappa R_{ij}), \quad (2)$$

where $R_{ij} = |\mathbf{R}_i - \mathbf{R}_j|$ and the location of particle $i(j)$ is $\mathbf{R}_{i(j)}$. The first term is a long-range Coulomb repulsion that will favor formation of a triangular lattice of particles in the absence of a substrate. For computational efficiency, we treat the long-range Coulomb interaction with a Lekner summation, as in previous work [2,50]. The second term is a short-range attraction that falls off exponentially. At very short range, the repulsive Coulomb interaction becomes dominant again, which prevents the particles from collapsing onto a point. In previous work [2,3,7,50,51], it was shown that particles with the interaction potential in Eq. (2) can form crystal, stripe, bubble, and void lattice states depending on the values of ρ, B, and κ. Here we fix $\kappa = 1.0$ and focus on a particle density of $\rho = 0.44$. In the absence of a substrate, this system forms a crystal for $B < 2.0$, a stripe state for $2.0 < B < 2.25$, and bubbles for $B > 2.25$. Adding a substrate and/or changing the particle density will modify the values of B for which these phases appear.

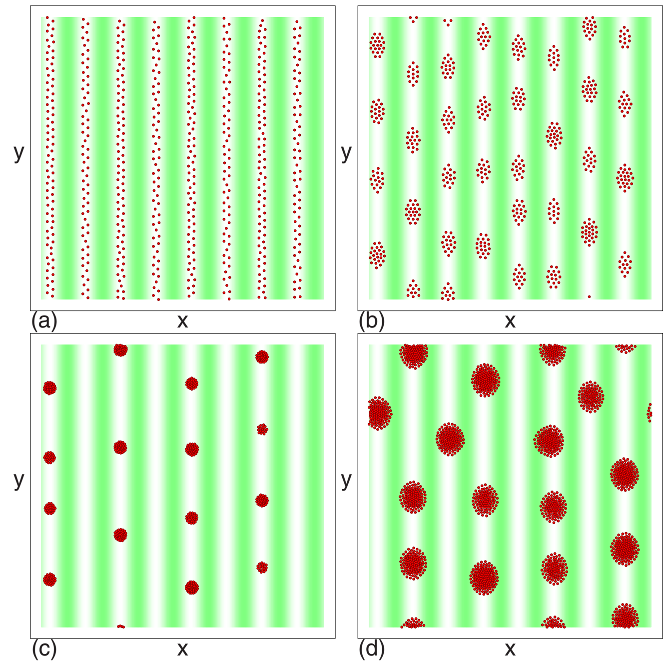

FIG. 1. The particle positions (red circles) and the q1D substrate potential (green shading) for a bubble-forming system at a particle density of $\rho = 0.44$ with a substrate lattice constant of $a_p = 4.5$ for $F_p = 2.0$ and $F_D = 0.0$. (a) A stripe state at $B = 2.25$. (b) A bubble phase at $B = 2.85$. (c) More compact bubbles at $B = 6.0$. (d) The $B = 2.85$ sample from (b) at $\rho = 1.38$, where larger bubbles appear.

The particles interact with a q1D substrate with N_p minima. The substrate force is given by

$$\mathbf{F}_s^i = F_p \cos(2\pi x_i/a_p), \quad (3)$$

where x_i is the x position of particle i and the spacing between substrate minima is $a_p = L/N_p$. Here we focus on substrates with $N_p = 8.0$, corresponding to $a_p = 4.5$.

We obtain the initial particle configuration by performing simulated annealing, where the particles are placed in an initial lattice, subjected to a high temperature, and then slowly cooled. The thermal forces are represented by Langevin kicks, and after the simulated annealing is complete, the temperature is set to zero. After the system has been initialized, we apply a driving force of $\mathbf{F}_D = F_D\hat{\mathbf{x}}$ to all of the particles and measure the time-averaged particle velocity in the direction of drive, $\langle V\rangle = \sum_i^N \mathbf{v}_i \cdot \hat{\mathbf{x}}$. We typically wait 10^5 or more time steps until the system has reached a steady state before taking data, and we average the velocity over a similar time frame. Due to the long-range interactions, the system can exhibit transient dynamics over relatively long time scales.

III. RESULTS

In Figs. 1(a)–1(c), we illustrate the particle positions and substrate potential for a system with $F_p = 2.0$, $\rho = 0.44$, and $a_p = 4.5$ at $F_D = 0.0$. For $B = 2.25$ in Fig. 1(a), the particles form stripes that are aligned with the substrate. In Fig. 1(b) at $B = 2.85$, bubbles appear that have an anisotropic shape due to the confinement from the substrate. At $B = 6.0$ in Fig. 1(c), the bubbles are much smaller and can fit better into

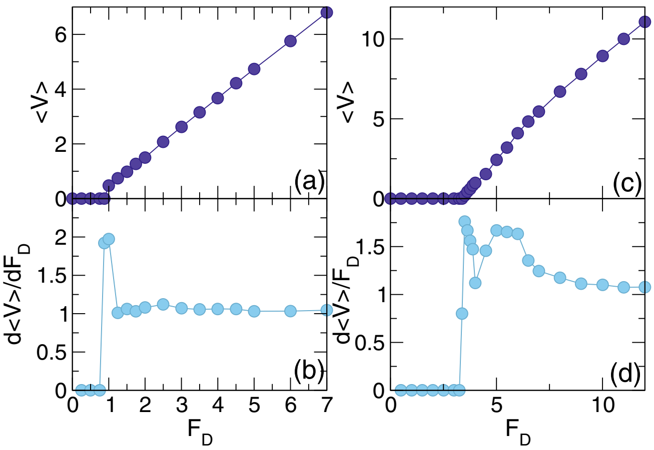

FIG. 2. (a) The average velocity per particle $\langle V\rangle$ vs F_D for the system in Fig. 1(b) with $a_p = 4.5$, $\rho = 0.44$, $B = 2.85$, and $F_p = 2.0$, where the depinning is elastic. (b) The corresponding $d\langle V\rangle/dF_D$ vs F_D curve. (c) $\langle V\rangle$ vs F_D for the same system but with $F_p = 5.0$, where the depinning is plastic. (d) The corresponding $d\langle V\rangle/dF_D$ vs F_D curve indicates that there is a two-step depinning process.

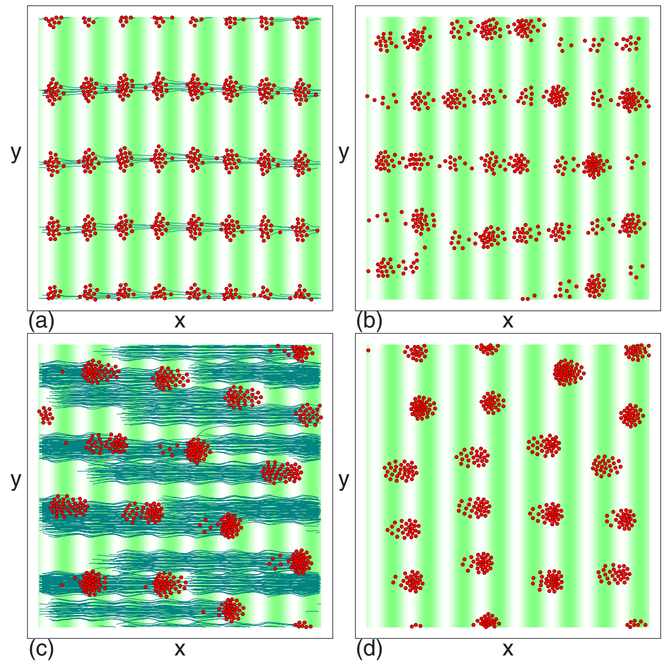

FIG. 3. The particle positions (red circles), trajectories (lines), and q1D substrate potential (green shading) for the system in Figs. 2(c), 2(d) with $a_p = 4.5$, $\rho = 0.44$, $B = 2.85$, and $F_p = 5.0$. (a) At $F_D = 3.75$ or $F_D/F_p = 0.75$, the bubbles are pinned, but individual particles are hopping from one bubble to the next. (b) At $F_D/F_p = 1.1$, all of the particles are moving but the bubble structure is disordered. For clarity, the trajectory lines are not shown. (c) At $F_D/F_p = 1.4$, organized bubbles reform but can shed and reabsorb individual particles, which are able to use the shedding mechanism to jump from one bubble to another. (d) At $F_D/F_p = 2.2$, the bubbles are fully formed and there is no shedding. For clarity, the trajectory lines are not shown. Videos of the motion in each panel appear in the Supplemental Material [53].

the sinusoidal substrate minima. Figure 1(d) shows the bubble phase sample with $B = 2.85$ from Fig. 1(b) at a higher particle density of $\rho = 1.38$, where the bubbles are more compact and each contains a larger number of particles.

We next focus on the depinning of the bubble phase for $B \geqslant 2.25$ by measuring the average velocity as a function of external drive for fixed $\rho = 0.44$ and $B = 2.85$. In Fig. 2(a), we plot the velocity-force curve for the system in Fig. 1(b). Near $F_D = 0.85$, the bubbles depin elastically, with all of the particles remaining in their original bubble both during the depinning process and at higher drives. Figure 2(b) shows that the corresponding $d\langle V\rangle/dF_D$ versus F_D curve has a sharp peak near depinning, while at higher drives the velocity-force curve becomes linear and $\langle V\rangle \propto F_D$. In systems that depin elastically, there is generally only a single peak in the differential velocity-force curves [52]. When we increase the substrate strength, we see a transition to plastic flow where the motion above depinning consists of individual particles hopping from one pinned bubble to the next, followed at higher drives by a state where moving bubbles shed and reabsorb individual particles as they travel through the system. In Figs. 2(c), 2(d) we plot the velocity-force and differential velocity-force curves for the same system from Fig. 2(a) but at $F_p = 5.0$, where the depinning is plastic. Here, there are two peaks in the differential velocity-force curve, and the velocity-force curve does not exhibit linear behavior until $F_D > 8.5$.

In Fig. 3(a), we show the particle locations and trajectories for the system in Figs. 2(c), 2(d) at $F_D = 3.75$, just above the first peak in the $d\langle V\rangle/dF_D$ curve. The system forms a rectangular lattice of pinned bubbles, and individual particles are able to hop from one bubble to the next. As F_D increases, the number of particles participating in this hopping process increases until $F_D/F_p > 1.0$, at which point all of the particles are able to move at the same time. When this happens, the bubble structure is partially broken up, as shown in Fig. 3(b) at $F_D/F_p = 1.1$. The second peak in the $d\langle V\rangle/F_D$ curve thus corresponds to the drive at which all of the particles become able to flow simultaneously. As F_D further increases, the bubble structure reassembles, as shown in Fig. 3(c) at $F_D/F_p = 1.4$, and each bubble can shed individual particles that proceed to jump from one moving bubble to another, where the particles are reabsorbed. In general, the individual particles move more slowly than the bubbles. For $F_D > 1.7$, the system forms a bubble lattice where the hopping process no longer occurs and all particles remain trapped within individual bubbles, as shown in Fig. 3(d) at $F_D/F_c = 2.2$. The bubble lattice formation occurs at the same drive that marks the transition to linear behavior of the velocity-force curve. In the moving bubble phase, the individual bubbles are anisotropic and are elongated in the driving direction.

The nonlinear velocity-force curve and the double peak feature in the differential velocity-force curve is a general feature of systems that exhibit plastic depinning [52]. In Figs. 4(a), 4(b) we plot the velocity-force and differential velocity-force curves for the system from Fig. 2 but at $F_p = 4.0$, while Figs. 4(c), 4(d) show $\langle V\rangle$ versus F_D and $d\langle V\rangle/F_D$ versus F_D for the same system at $F_p = 6.0$, where the multiple peak feature in $d\langle V\rangle/F_D$ is even more pronounced. From the images and the features in the transport curves, we can identify four dynamical phases that appear as a function of

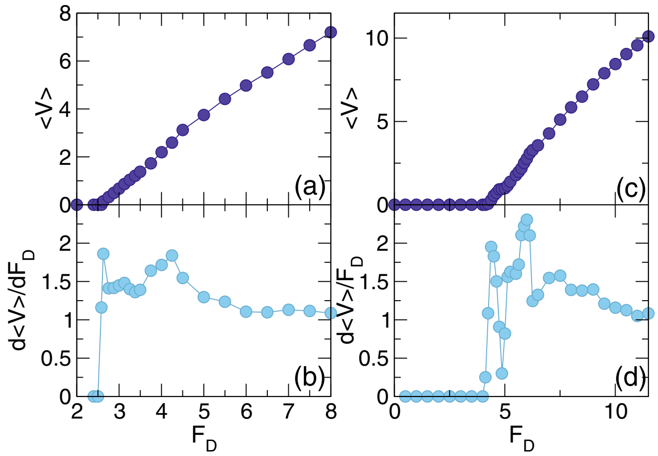

FIG. 4. (a) $\langle V\rangle$ vs F_D for the system from Fig. 2 with $a_p = 4.5$, $\rho = 0.44$, and $B = 2.85$ but at $F_p = 4.0$. (b) The corresponding $d\langle V\rangle/dF_D$ vs F_D curve showing a multiple step depinning process. (c) $\langle V\rangle$ vs F_D for the same system but with $F_p = 6.0$. (d) The corresponding $d\langle V\rangle/dF_D$ vs F_D curve.

applied drive and substrate strength. These are: a pinned bubble phase where the velocity is zero; an intrabubble hopping phase where the bubbles are pinned but individual particles can hop from one bubble to the next; a disordered moving partial bubble phase where all of the particles are moving but the bubble structure has been disrupted by a shedding and reabsorption process; and a high drive elastically moving bubble lattice.

In Fig. 5(a), we show the depinning threshold F_c versus pinning strength F_p for the system in Figs. 2 and 4, while Fig. 5(b) shows the corresponding dF_c/dF_p versus F_p curve. The depinning is elastic for $F_p < 2.25$ and plastic for $F_p \geqslant 2.25$. The elastic-to-plastic transition is marked by a jump

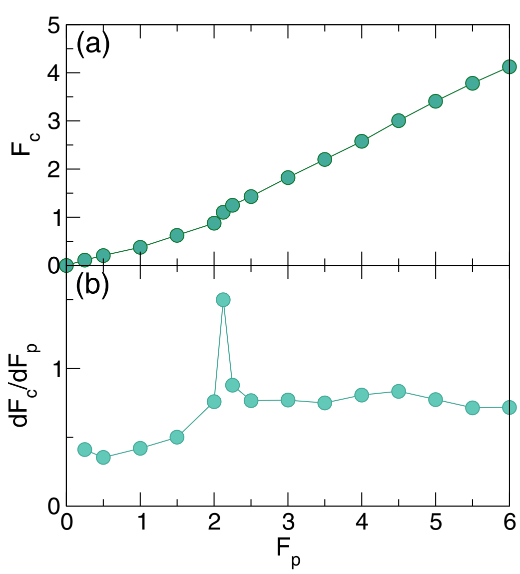

FIG. 5. (a) The depinning force F_c vs F_p for the system in Figs. 2 and 4 with $a_p = 4.5$, $\rho = 0.44$, and $B = 2.85$. (b) The corresponding dF_c/dF_p vs F_p curve. The peak corresponds to the transition from elastic depinning to plastic depinning with increasing F_p.

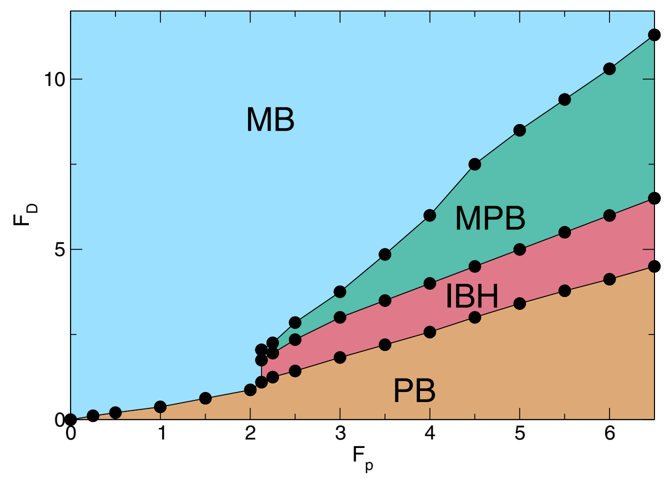

FIG. 6. Dynamic phase diagram as a function of F_D vs F_P for the system from Fig. 4 with $a_p = 4.5$, $\rho = 0.44$, and $B = 2.85$, where we highlight the moving bubble lattice (MB) phase, an intrabubble hopping (IBH) phase, a moving partial bubble (MPB) phase, and a pinned bubble (PB) phase.

up in the depinning force and a peak in dF_c/dF_p. A sharp increase in the depinning threshold at the transition from elastic-to-plastic behavior has been well studied in other systems with random or periodic substrates that exhibit depinning phenomena [52]. Additionally, for $F_p \geqslant 2.25$, we find that the depinning threshold increases linearly according to $F_c \approx F_p$, as expected for plastic depinning [52].

From the particle structures and the features in the transport curves, we can construct a dynamical phase diagram highlighting the different dynamical regimes, as shown in Fig. 6 as a function of F_D versus F_p for the system from Figs. 2 and 4. For $F_p < 2.25$, there is an elastic depinning transition directly from a pinned bubble (PB) lattice to a moving bubble (MB) lattice, while for $F_p \geqslant 2.25$, an initial depinning transition takes the system into the intrabubble hopping (IBH) phase, a second depinning transition results in the appearance of the disordered moving partial bubble (MPB) phase, and at higher drives a dynamic reordering transition occurs into the moving bubble (MB) lattice. Dynamical ordering at high drives in systems with plastic depinning transitions has been observed in systems with both random and ordered substrates [52].

IV. EFFECT OF BUBBLE SIZE ON DYNAMICS

We next consider the effect of changing the strength B of the attractive interaction term. For larger B, the bubbles shrink in size and become more rigid, as shown in Fig. 1(c). We note that individual bubbles can capture an increased number of particles even as the bubble radius decreases with increasing B; however, because the Coulomb interaction becomes dominant again at small length scales, the particles are unable to assemble into a single large bubble but instead form a collection of bubbles.

We first consider the case for $F_p = 2.0$, where the depinning transition is elastic. In Fig. 7, we plot $\langle V\rangle$ versus B in a sample with $\rho = 0.44$ and $F_p = 0.1$ at $F_D = 0.875$, 1.0, 1.125, 1.25, 1.375, 1.5, 1.625, 1.75, 1.875, 2.0, and 2.25.

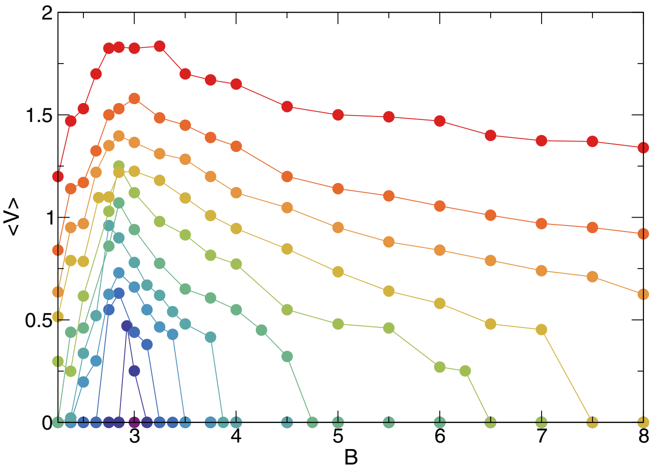

FIG. 7. $\langle V \rangle$ vs B for a system with $a_p = 4.5$, $\rho = 0.44$, and $F_p = 0.1$ at $F_D = 0.875$, 1.0, 1.125, 1.25, 1.375, 1.5, 1.625, 1.75, 1.875, 2.0, and 2.25, from bottom to top. Here, $\langle V \rangle$ is nonmonotonic, and there is a reentrant pinning transition at higher B.

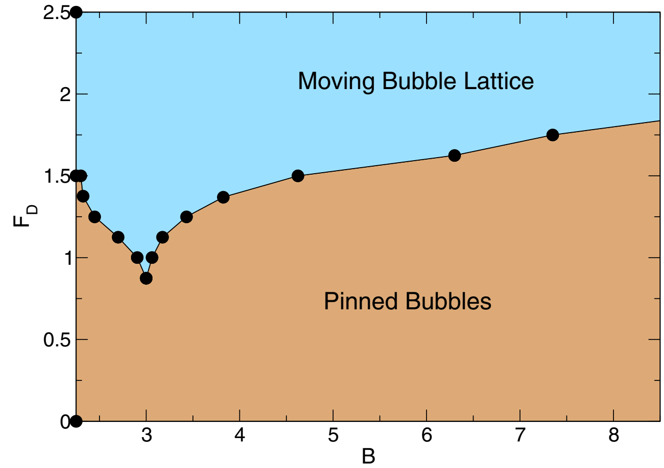

FIG. 8. Dynamic phase diagram as a function of F_D vs B showing the pinned bubble and moving bubble lattice regimes for the system in Fig. 7 with $a_p = 4.5$, $\rho = 0.44$, and $F_p = 0.1$. A dip appears near $B = 3.0$ where the bubbles are less well pinned.

When $F_D < 1.375$, the velocity drops to zero for low values of B. In this low-B pinned state, a strongly pinned stripe phase appears, and the depinning and sliding dynamics of this stripe phase will be described in a separate paper. For each value of F_D, $\langle V \rangle$ has a nonmonotonic dependence on B, with a maximum appearing near $B = 3.0$ followed by a velocity decrease. When $F_D < 1.875$, at higher B the velocity drops completely to zero, indicating that the bubbles have become pinned. This result indicates that there can be both a low-B pinned state and a high-B reentrant pinned state.

The nonmonotonic behavior of the velocity and the reentrant pinning occur because of two effects: the ability of the bubble to distort, and the change in size of the bubble. For $B < 3.0$, the bubbles are large but can partially distort to fit inside the pinning troughs as elongated or anisotropic bubbles. As B increases, the bubbles shrink but also become stiffer, and are thus less able to accommodate anisotropic distortions. Near $B = 3.0$, the bubbles become too round to elongate enough to fit completely into an individual pinning trough, reducing the effectiveness of the pinning. For $B > 3.0$, the bubbles remain round, but the bubble radius decreases, as shown in Fig. 1(c). These smaller bubbles can fit more easily into the pinning troughs, increasing the effectiveness of the pinning, and the system starts to act more like a lattice of point particles. Thus, the smaller bubbles are better pinned even when the number of particles in each individual bubble remains the same. In Fig. 8, we plot a dynamic phase diagram as a function of F_D versus B showing the pinned bubbles and moving bubble lattice phases. A dip in the transition point appears near $B = 3.0$, where the pinning effectiveness of the substrate is the most greatly reduced by the shape of the bubbles. For $B \leqslant 2.25$, the system forms a moving stripe phase.

In Fig. 9 we plot $\langle V \rangle$ versus B for the same system from Fig. 7 but with $F_p = 5.0$ at $F_D = 3.5$, 4.0, and 5.0. For this system, the depinning is plastic for $B < 3.25$ and elastic for $B \geqslant 3.25$. The velocities are lower within the plastic or IBH regime and show a jump up at the entrance to the elastic regime, with a peak velocity appearing near $B = 3.25$ followed by a velocity drop at larger B as the bubble size decreases. There is a reentrant pinning regime at high values of B. The smaller bubbles are less likely to undergo plastic deformations or permit bubble-to-bubble hopping because the attractive interaction forces generate a greater barrier for individual particles to jump out of a bubble. From the flow patterns and the features in the transport curves, in Fig. 10 we construct a dynamic phase diagram for the system in Fig. 9 as a function of F_D versus B. The depinning force is lowest near $B = 3.5$, close to the elastic to plastic transition, and the drive that must be applied to the plastic phase in order to dynamically reorder the system increases with decreasing B. As B increases in the elastic regime, the depinning threshold increases because the bubble size is diminishing.

Another way to characterize the plastic and elastic flow regimes is to measure the power spectra of the velocity noise

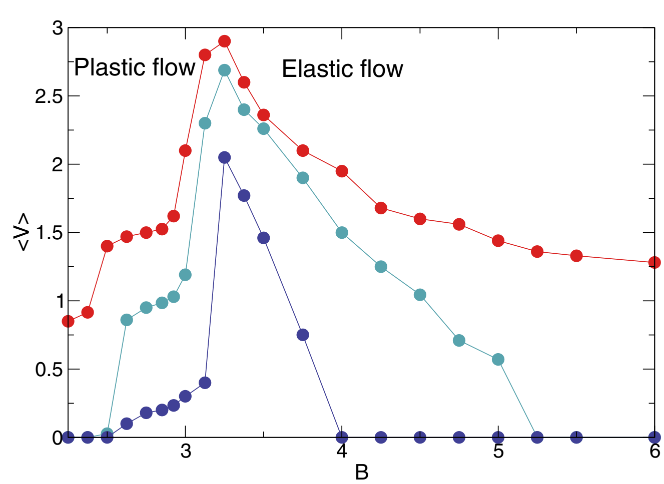

FIG. 9. $\langle V \rangle$ vs B for the system from Fig. 7 with $a_p = 4.5$ and $\rho = 0.44$ at $F_p = 5.0$ for $F_D = 3.5$, 4.0, and 5.0, from bottom to top. The depinning is plastic for $B < 3.25$ and elastic for $B \geqslant 3.25$, and there is a reentrant pinning regime at high B.

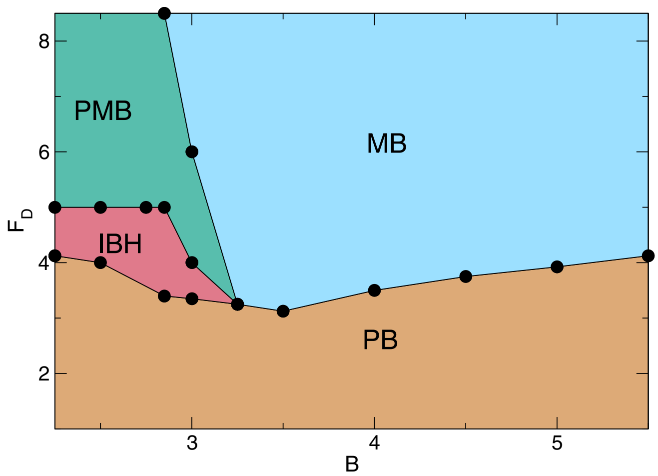

FIG. 10. Dynamic phase diagram as a function of F_D vs B for the system in Fig. 9 with $a_p = 4.5$, $\rho = 0.44$, and $F_p = 5.0$ showing the pinned bubble (PB) phase, intrabubble hopping (IBH) phase, moving partial bubble (MPB) phase, and elastic moving bubble (MB) phase.

fluctuations from time series data. In Fig. 11(a), we plot the time-dependent velocity for the system in Figs. 9 and 10 at $B = 2.75$, which corresponds to the interbubble hopping plastic flow phase where the velocity signal has no significant features. We also plot V as a function of time for a sample with $B = 3.5$ in the moving bubble phase, where there is a strong periodic velocity signal consistent with the washboard signature expected for an elastic solid moving over a periodic potential. Figure 11(b) shows the power spectra $S(\omega) = |\sum V(t)e^{-i\omega t}|^2$ for the two velocity signals. In the intrabubble hopping phase, there is $1/f$ noise at lower frequencies, while a strong narrow band noise signal appears for the moving bubble phase. This indicates that moving bubbles should produce a washboard signal, while the intrabubble hopping flow is more disordered. We find similar noise features for plastic versus elastic flow for other parameters.

To further explore how the bubble size affects the pinning effectiveness, we consider a substrate with a smaller lattice constant at the same particle density and the same range of B values. In Fig. 12 we plot $\langle V\rangle$ versus B for a system with $\rho = 0.44$, fixed $F_D = 0.5$, and a substrate lattice constant of

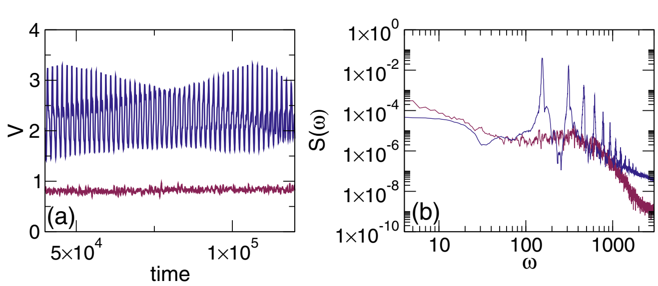

FIG. 11. Velocity time series V vs time for the system in Fig. 10 with $a_p = 4.5$, $\rho = 0.44$, $F_p = 5.0$, and $F_D = 4.0$ at $B = 2.75$ (red) in the IBH or plastic flow phase and $B = 3.5$ (blue) in the moving bubble lattice or MB phase. There is a strong time periodic signal in the MB phase. (b) The corresponding power spectra $S(\omega)$ shows strong peaks in the moving bubble phase.

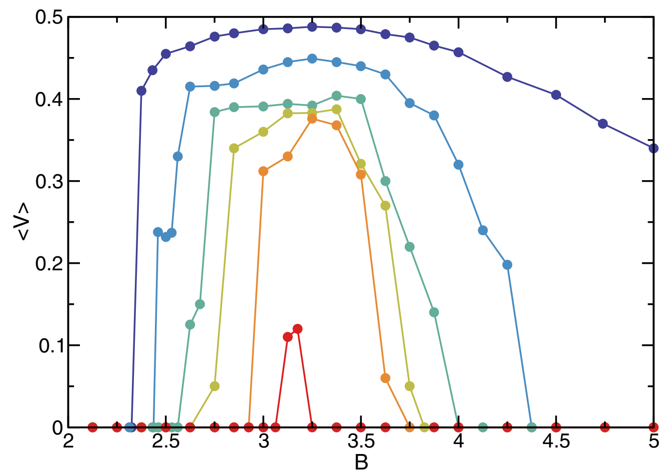

FIG. 12. $\langle V\rangle$ vs B for a system with $F_D = 0.5$, $\rho = 0.44$, and a smaller pinning lattice constant of $a_p = 2.11$ for $F_p = 1.0$, 2.0, 3.0, 4.0, 5.0, and 6.0, from top to bottom. At low B, the system forms a pinned stripe phase as illustrated in Fig. 13(a) for $B = 2.25$ and $F_p = 2.0$. When the velocity becomes finite, the system depins plastically into the sliding bubble track phase shown in Fig. 13(b) for $B = 2.5$ and $F_p = 2.0$. At high velocities, the system forms a bubble phase where the bubbles are close to twice the size of the pinning lattice constant, as shown in Fig. 13(c) for $B = 2.75$ and $F_p = 2.0$. For higher B, the system reenters a pinned state when the bubbles become small enough to fit inside a single pinning trough, as shown in Fig. 13(d) for $B = 4.5$ and $F_p = 2.0$.

$a_p = 2.11$, half as large as what was used for the results presented up to this point, at substrate strengths of $F_p = 2.0$, 3.0, 4.0, 5.0, and 6.0. For $F_p = 2.0$, the system is pinned when $B < 2.4375$, and the particles form a 1D stripelike pattern as shown in Fig. 13(a) for $B = 2.25$. A new plastic flow state, distinct from that illustrated earlier, appears for $2.4375 < B < 2.6$, where the system forms the sliding bubble track phase illustrated in Fig. 13(b) at $B = 2.5$. Here, pinned particles remain trapped in stripes that form tracks parallel to the driving direction, and the bubbles travel along these pinned tracks. For $B \geqslant 2.6$, the system forms a moving bubble lattice, as shown in Fig. 13(c) at $B = 2.75$, where it can be seen that when the bubbles form, they do not fit into the substrate troughs. The transition to the moving bubble lattice occurs at the large jump up in $\langle V\rangle$ in Fig. 12. As F_p is varied, the same phases appear for shifted values of B.

In general, the bubbles are less strongly pinned for the smaller substrate lattice spacing because the size of the bubbles is larger than the width of the substrate troughs, causing the bubbles to sit partially on the potential maxima separating adjacent pinning troughs. As B increases, the bubbles shrink, and the velocity goes to zero when B becomes large enough to permit each bubble to fit entirely within a single substrate trough, as shown in Fig. 13(d) for $B = 4.5$. When the driving force is fixed to $F_D = 0.5$, the moving bubble phase continues to flow as the pinning force increases up until $F_p = 6.0$, when the bubbles become pinned. In Fig. 14, we construct a dynamic phase diagram as a function of F_p versus B for the system in Fig. 12, highlighting the regime in which the moving bubble lattice can occur. For $B < 3.0$,

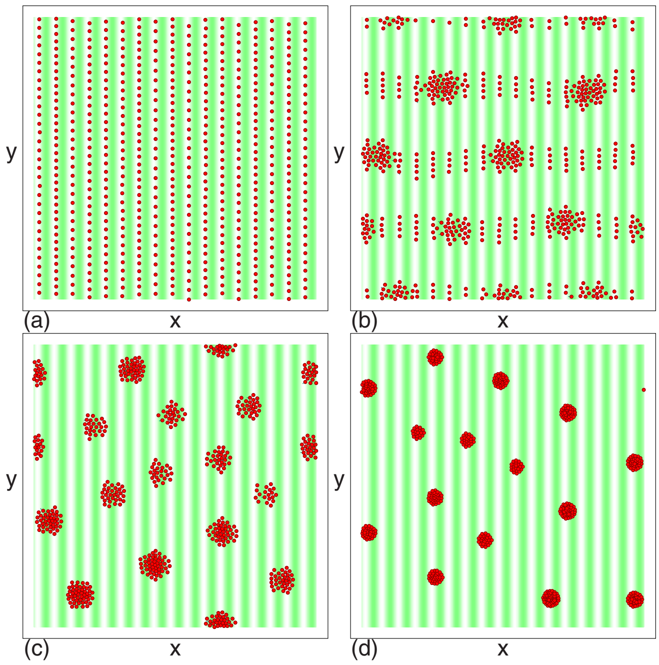

FIG. 13. The particle positions (red circles) and q1D substrate potential (green shading) for the system in Fig. 12 with $a_p = 2.11$, $\rho = 0.44$, $F_p = 2.0$, and $F_D = 0.5$. (a) A pinned stripe phase at $B = 2.25$. (b) A plastic sliding bubble track phase at $B = 2.5$. Pinned particles form stripe tracks and the bubbles move along these stripe tracks. (c) A moving bubble phase at $B = 2.75$ where the bubble size is greater than the width of the substrate troughs. (d) A pinned bubble lattice at $B = 4.5$ where the bubbles are small enough to fit within individual pinning troughs. Videos of the motion in (b) and (c) appear in the Supplemental Material [53].

the pinned phase consists of a strongly anisotropic bubble or stripe arrangement, while for $B > 3.0$, the system forms a pinned bubble lattice. We note that right along the boundary between the pinned anisotropic bubble/stripe state and the moving bubble state, the system is in the plastic sliding bubble track phase, which is too narrow to highlight in the diagram.

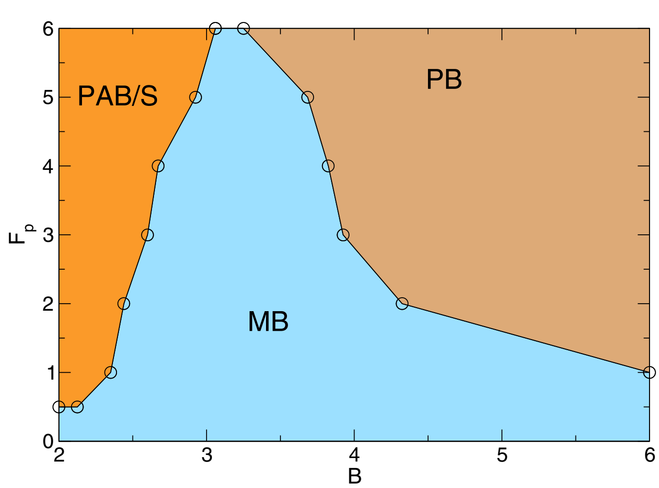

FIG. 14. Dynamic phase diagram as a function of F_p vs B for the system in Fig. 12 with $F_D = 0.5$, $\rho = 0.44$, and $a_p = 2.11$ showing the pinned anisotropic bubble/stripe phase (PAB/S), the moving bubble lattice (MB), and the pinned bubble lattice (PB) that appears for higher B.

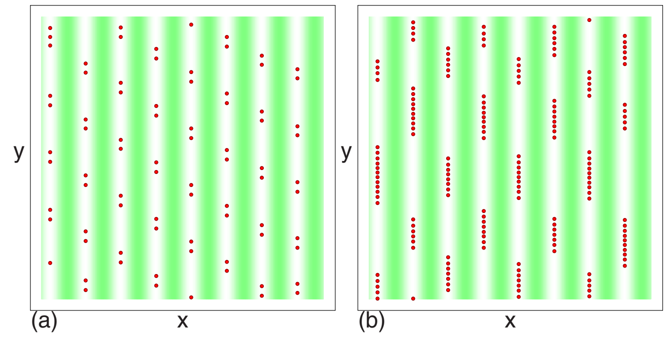

FIG. 15. The particle positions (red circles) and q1D substrate potential (green shading) for low particle density systems with $F_p = 4.0$, $a_p = 4.5$, and $B = 2.85$ at $F_D = 0$. (a) A dimer lattice at $\rho = 0.0617$. (b) A stripe bubble lattice at $\rho = 0.126$.

To further demonstrate that the larger bubbles are less well pinned, we fix $B = 2.85$ while increasing the particle density in order to produce large bubbles similar to those shown in Fig. 1(d). In general, we find that smaller particle densities result in higher effective pinning. In Figs. 15(a), 15(b) we show the bubble configurations for a system with $a_p = 4.5$ and $F_p = 4.0$ at lower particle densities, where we find a dimer bubble state for $\rho = 0.0617$ and a latticelike arrangement of 1D stripes at $\rho = 0.126$. In general, the 1D-like structures are more strongly pinned than the 2D bubble phases that form at higher particle densities. In Fig. 16 we plot $\langle V \rangle$ versus ρ for a system with $F_p = 4.0$, $a_p = 4.5$, and $B = 2.85$ at $F_D = 2.0, 2.5, 3.0, 3.5, 4.0, 4.5,$ and 5.0. When $F_D < 4.0$ and $\rho < 0.75$, the system is a pinned 1D bubble state similar to those illustrated in Fig. 15. In general, the average particle velocity increases with increasing ρ as the bubbles become larger.

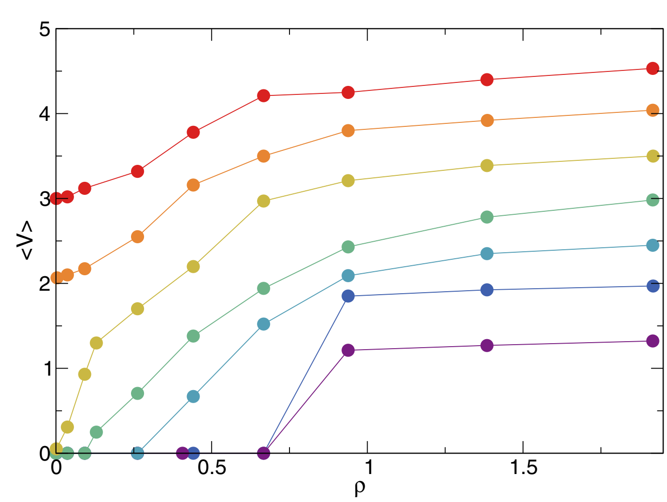

FIG. 16. $\langle V \rangle$ vs ρ for a system with $F_p = 4.0$, $a_p = 4.5$, and $B = 2.85$ at $F_D = 2.0, 2.5, 3.0, 3.5, 4.0, 4.5,$ and 5.0, from bottom to top, showing a general increase in the velocity with increasing ρ as the bubbles grow in size. The system is more strongly pinned for the lower densities, where 1D anisotropic structures appear.

V. DISCUSSION

As we have shown, the bubble states exhibit distinct phenomena beyond what appears for lattices of individual particles depinning from periodic one-dimensional substrates. The bubbles have both a finite size and internal degrees of freedom that are lacking for individual pointlike particles. For particle-based models of systems with purely repulsive particle-particle interactions, such as superconducting vortices or Wigner crystals, there can be either elastic flow where all of the particles maintain their same neighbors, or plastic flow in which certain particles remain pinned while other particles move past them. The bubble system exhibits an elastic depinning transition similar to that found for the pointlike particle models, but also exhibits quite distinct plastic depinning regimes in which the bubbles break apart either partially or completely. Plastic flow for the bubble system can occur via individual particles hopping from one bubble to the next or via the motion of bubbles accompanied by shedding of individual particles. These types of plastic flow do not occur for purely repulsive pointlike particles, and the distinctive bubble plastic flow phases produce measurable features in the transport curves.

The size and flexibility of the bubbles also play an important role in the dynamical behavior. For example, we demonstrate that softer bubbles are better pinned than stiff bubbles since the soft bubbles can deform in order to take greater advantage of the pinning energy. We also show that the size of the bubbles matters, leading to a nonmonotonic depinning threshold as a function of the strength of the attractive term. In general, bubbles are less strongly pinned than stripes as the attractive term becomes larger, since the number of particles in the bubble increases with increasing attraction and larger bubbles do not fit as well into the pinning troughs. At the same time, the bubble radius decreases as the attractive term increases, so that even though there may be a greater number of particles in a bubble for large attraction, the bubble size may decrease overall. These smaller-sized bubbles are better pinned since they fit better into the bottom of the pinning trough. This leads to the unexpected nonmonotonicity of the depinning threshold, since the smaller bubbles are more strongly pinned and produce a reentrant pinning effect for increasing attraction. This holds true even for bubbles with a larger number of particles.

A variety of systems could exhibit behavior similar to that studied in this work. These include the bubble phases that are expected to arise in electron liquid systems subjected to a magnetic field and interacting with a periodic one-dimensional potential. Here, the number of particles in the bubble could be tuned by varying the magnetic field. An example of a prediction from our work for this system is that bubble phases should have a lower pinning threshold than stripe states. Another possible realization is the vortex bubble phases observed in low-κ superconductors near an intermediate regime for samples in which the vortices are coupled to a periodic q1D substrate. In this case, the bubble size and particle number are also controlled by varying the magnetic field. Other possible realizations could be achieved in soft matter systems, such as charged colloids with some form of attraction that also interact with periodic substrates.

There are many further directions to study in this system. For example, the plastic flow we observe consists of bubble-to-bubble hopping, so the bubbles have to break apart; however, there could also be plastic flow states in which individual bubbles remain intact, but some bubbles remain pinned while others move, similar to the plastic flow observed in nonbubble particlelike systems. We expect that this type of bubble lattice plasticity could appear in systems where the pinning substrate is more heterogeneous. We have only considered external driving applied parallel to the substrate modulation direction or x axis, but the drive could be applied at angles with respect to the x axis, which would likely produce a combination of sliding along the y direction and hopping in the x direction. The depinning forces could also exhibit commensuration effects based on how well the bubble size matches the substrate lattice spacing, so that bubbles whose radii are integer multiples of the substrate lattice constant are more strongly pinned. We have only considered dc driving, but if the dc drive were combined with ac driving, we would expect additional Shapiro steplike phenomena to arise, especially in the sliding bubble lattice state where there is a strong washboard frequency. Shapiro steps in the velocity-force curve arise when an ac drive is superimposed on a dc drive in such a way that the frequency of the ac drive matches the periodic washboard velocity signals generated when the particles move over a periodic substrate [54–59]. In the case considered here, additional step features can appear due to the presence of additional internal frequencies associated with the motion of the particles composing an individual bubble. This could produce additional steps in the velocity-force curves beyond the steps associated solely with the washboard frequency. If thermal effects were included, it is likely that the intrabubble hopping phase would develop an extended range of creeplike behavior, and all of the depinning thresholds would shift to lower values. In this case, it would be interesting to compare intrabubble creep with bubble lattice creep.

If the interaction potential of Eq. (2) were replaced by a different form of interaction, we expect that many of our results would remain robust, such as the dependence of the depinning threshold on the bubble size and the observation of particles hopping from bubble to bubble, but that some of the phases we describe could appear in an expanded regime. For example, in the case of colloidal systems where the long-range interactions would be cut off due to screening, we think there would be an enhancement of the regime in which particles hop from one bubble to another since the longer-range barriers to motion would be reduced. For a system with shorter-range repulsion, if the bubble density is low, then a bubble lattice structure may not occur but could be replaced by a more disordered bubble state. For denser bubble arrays, however, bubble lattices should appear even for shorter-range repulsive interaction potentials.

VI. SUMMARY

We have investigated a pattern-forming system of particles with competing long-range repulsion and short-range attraction driven over quasi-one-dimensional periodic substrates, and have focused on the bubble regime. For a fixed driving force, stripe states are strongly pinned because they can align with the pinning troughs. In the bubble phase, there can be elastic depinning, where the moving bubbles maintain their original complement of particles and the differential velocity force curves show only a single peak, or plastic depinning, where individual particles hop from one pinned bubble to an adjacent pinned bubble. In the plastic depinning regime, the differential velocity force curves exhibit two peaks, with the second peak corresponding to the drive at which all of the bubbles begin to flow but the motion remains plastic since individual bubbles continuously shed and reabsorb particles. At higher drives, the system can dynamically reorder into a moving bubble lattice where no particle shedding occurs. When the pinning substrate lattice constant is reduced, we also find a plastic sliding bubble track phase in which a portion of the particles form tracks consisting of pinned stripes oriented with the driving direction, and the remaining particles form bubbles that move over the tracks. The effectiveness of the pinning, which is visible in both the depinning threshold and the velocity of the moving bubbles, depends on the size and flexibility of the individual bubbles. When the attractive interaction term is weak and the bubbles are highly flexible, the bubbles can distort anisotropically in order to fit between the pinning troughs and become better pinned. Increasing the attractive interaction term stiffens the bubbles, making them more round in shape, but also shrinks their radius. The stiffer bubbles cannot accommodate themselves to the shape of the pinning troughs, but once the bubbles drop below the width of the pinning troughs, they can be well pinned by the substrate. This leads to a nonmonotonic dependence of the velocity on the strength of the attractive interaction term, where there is a pinned state for flexible bubbles that can distort into stripelike shapes, as well as a reentrant pinned state that appears when the size of an individual bubble decreases enough that it can fit inside a pinning trough. Our results should be relevant to a variety of bubble-forming systems, including electron bubbles, colloidal particles, and magnetic skyrmions.

ACKNOWLEDGMENTS

We gratefully acknowledge the support of the U.S. Department of Energy through the LANL/LDRD program for this work. This work was supported by the U.S. Department of Energy through the Los Alamos National Laboratory. Los Alamos National Laboratory is operated by Triad National Security, LLC, for the National Nuclear Security Administration of the U.S. Department of Energy (Contract No. 892333218NCA000001).

[1] S. Mossa, F. Sciortino, P. Tartaglia, and E. Zaccarelli, Ground-state clusters for short-range attractive and long-range repulsive potentials, Langmuir **20**, 10756 (2004).

[2] C. Reichhardt, C. J. Olson, I. Martin, and A. R. Bishop, Depinning and dynamics of systems with competing interactions in quenched disorder, Europhys. Lett. **61**, 221 (2003).

[3] C. J. O. Reichhardt, C. Reichhardt, I. Martin, and A. R. Bishop, Dynamics and melting of stripes, crystals, and bubbles with quenched disorder, Physica D **193**, 303 (2004).

[4] F. Sciortino, S. Mossa, E. Zaccarelli, and P. Tartaglia, Equilibrium cluster phases and low-density arrested disordered states: The role of short-range attraction and long-range repulsion, Phys. Rev. Lett. **93**, 055701 (2004).

[5] K. Nelissen, B. Partoens, and F. M. Peeters, Bubble, stripe, and ring phases in a two-dimensional cluster with competing interactions, Phys. Rev. E **71**, 066204 (2005).

[6] Y. H. Liu, L. Y. Chew, and M. Y. Yu, Self-assembly of complex structures in a two-dimensional system with competing interaction forces, Phys. Rev. E **78**, 066405 (2008).

[7] C. J. Olson Reichhardt, C. Reichhardt, and A. R. Bishop, Structural transitions, melting, and intermediate phases for stripe- and clump-forming systems, Phys. Rev. E **82**, 041502 (2010).

[8] L. Q. Costa Campos, S. W. S. Apolinario, and H. Löwen, Structural ordering of trapped colloids with competing interactions, Phys. Rev. E **88**, 042313 (2013).

[9] H. J. Zhao, V. R. Misko, and F. M. Peeters, Dynamics of self-organized driven particles with competing range interaction, Phys. Rev. E **88**, 022914 (2013).

[10] E. A. Jagla, Phase behavior of a system of particles with core collapse, Phys. Rev. E **58**, 1478 (1998).

[11] G. Malescio and G. Pellicane, Stripe phases from isotropic repulsive interactions, Nature Mater. **2**, 97 (2003).

[12] A. Imperio and L. Reatto, Microphase separation in two-dimensional systems with competing interactions, J. Chem. Phys. **124**, 164712 (2006).

[13] M. A. Glaser, G. M. Grason, R. D. Kamien, A. Kosmrlj, C. D. Santangelo, and P. Ziherl, Soft spheres make more mesophases, Europhys. Lett. **78**, 46004 (2007).

[14] E. Babaev and M. Speight, Semi-Meissner state and neither type-I nor type-II superconductivity in multicomponent superconductors, Phys. Rev. B **72**, 180502(R) (2005).

[15] V. Moshchalkov, M. Menghini, T. Nishio, Q. H. Chen, A. V. Silhanek, V. H. Dao, L. F. Chibotaru, N. D. Zhigadlo, and J. Karpinski, Type-1.5 superconductivity, Phys. Rev. Lett. **102**, 117001 (2009).

[16] A. Chaves, L. Komendová, M. V. Milošević, J. S. Andrade, G. A. Farias, and F. M. Peeters, Conditions for nonmonotonic vortex interaction in two-band superconductors, Phys. Rev. B **83**, 214523 (2011).

[17] X. B. Xu, H. Fangohr, S. Y. Ding, F. Zhou, X. N. Xu, Z. H. Wang, M. Gu, D. Q. Shi, and S. X. Dou, Phase diagram of vortex matter of type-II superconductors, Phys. Rev. B **83**, 014501 (2011).

[18] K. A. H. Sellin and E. Babaev, Stripe, gossamer, and glassy phases in systems with strong nonpairwise interactions, Phys. Rev. E **88**, 042305 (2013).

[19] L. Komendová, M. V. Milošević, and F. M. Peeters, Soft vortex matter in a type-I/type-II superconducting bilayer, Phys. Rev. B **88**, 094515 (2013).

[20] Q. Meng, C. N. Varney, H. Fangohr, and E. Babaev, Phase diagrams of vortex matter with multi-scale inter-vortex interactions in layered superconductors, J. Phys.: Condens. Matter **29**, 035602 (2017).

[21] J. F. Neto and C. C. de Souza Silva, Mesoscale phase separation of skyrmion-vortex matter in chiral-magnet–superconductor heterostructures, Phys. Rev. Lett. **128**, 057001 (2022).
[22] M. M. Fogler, A. A. Koulakov, and B. I. Shklovskii, Ground state of a two-dimensional electron liquid in a weak magnetic field, Phys. Rev. B **54**, 1853 (1996).
[23] R. Moessner and J. T. Chalker, Exact results for interacting electrons in high Landau levels, Phys. Rev. B **54**, 5006 (1996).
[24] K. B. Cooper, M. P. Lilly, J. P. Eisenstein, L. N. Pfeiffer, and K. W. West, Insulating phases of two-dimensional electrons in high Landau levels: Observation of sharp thresholds to conduction, Phys. Rev. B **60**, R11285 (1999).
[25] E. Fradkin and S. A. Kivelson, Liquid-crystal phases of quantum Hall systems, Phys. Rev. B **59**, 8065 (1999).
[26] B. Friess, V. Umansky, K. von Klitzing, and J. H. Smet, Current flow in the bubble and stripe phases, Phys. Rev. Lett. **120**, 137603 (2018).
[27] V. Shingla, H. Huang, A. Kumar, L. N. Pfeiffer, K. W. West, K. W. Baldwin, and G. A. Csáthy, A highly correlated topological bubble phase of composite fermions, Nature Phys. **19**, 689 (2023).
[28] M. Seul and D. Andelman, Domain shapes and patterns - the phenomenology of modulated phases, Science **267**, 476 (1995).
[29] A. D. Stoycheva and S. J. Singer, Stripe melting in a two-dimensional system with competing interactions, Phys. Rev. Lett. **84**, 4657 (2000).
[30] P. J. Camp, Structure and phase behavior of a two-dimensional system with core-softened and long-range repulsive interactions, Phys. Rev. E **68**, 061506 (2003).
[31] W. Jiang, P. Upadhyaya, W. Zhang, G. Yu, M. B. Jungfleisch, F. Y. Fradin, J. E. Pearson, Y. Tserkovnyak, K. L. Wang, O. Heinonen, S. G. E. te Velthuis, and A. Hoffmann, Blowing magnetic skyrmion bubbles, Science **349**, 283 (2015).
[32] K. Dholakia, G. Spalding, and M. MacDonald, Optical tweezers: the next generation, Phys. World **15**, 31 (2002).
[33] C. Reichhardt and C. J. Olson, Novel colloidal crystalline states on two-dimensional periodic substrates, Phys. Rev. Lett. **88**, 248301 (2002).
[34] M. Brunner and C. Bechinger, Phase behavior of colloidal molecular crystals on triangular light lattices, Phys. Rev. Lett. **88**, 248302 (2002).
[35] A. Gopinathan and D. G. Grier, Statistically locked-in transport through periodic potential landscapes, Phys. Rev. Lett. **92**, 130602 (2004).
[36] J. Mikhael, M. Schmiedeberg, S. Rausch, J. Roth, H. Stark, and C. Bechinger, Proliferation of anomalous symmetries in colloidal monolayers subjected to quasiperiodic light fields, Proc. Natl. Acad. Sci. USA **107**, 7214 (2010).
[37] M. P. N. Juniper, A. V. Straube, D. G. A. L. Aarts, and R. P. A. Dullens, Colloidal particles driven across periodic optical-potential-energy landscapes, Phys. Rev. E **93**, 012608 (2016).
[38] R. L. Stoop, A. V. Straube, T. H. Johansen, and P. Tierno, Collective directional locking of colloidal monolayers on a periodic substrate, Phys. Rev. Lett. **124**, 058002 (2020).
[39] J. Chakrabarti, H. R. Krishnamurthy, A. K. Sood, and S. Sengupta, Reentrant melting in laser field modulated colloidal suspensions, Phys. Rev. Lett. **75**, 2232 (1995).
[40] Q.-H. Wei, C. Bechinger, D. Rudhardt, and P. Leiderer, Experimental study of laser-induced melting in two-dimensional colloids, Phys. Rev. Lett. **81**, 2606 (1998).
[41] C. Bechinger, M. Brunner, and P. Leiderer, Phase behavior of two-dimensional colloidal systems in the presence of periodic light fields, Phys. Rev. Lett. **86**, 930 (2001).
[42] J. Baumgartl, M. Brunner, and C. Bechinger, Locked-floating-solid to locked-smectic transition in colloidal systems, Phys. Rev. Lett. **93**, 168301 (2004).
[43] C. Reichhardt and C. J. O. Reichhardt, Pinning and dynamics of colloids on one-dimensional periodic potentials, Phys. Rev. E **72**, 032401 (2005).
[44] F. Bürzle and P. Nielaba, Phase transitions in two-dimensional model colloids in a one-dimensional external potential, Phys. Rev. E **76**, 051112 (2007).
[45] P. Tierno, T. M. Fischer, T. H. Johansen, and F. Sagués, Colloidal assembly on magnetically vibrated stripes, Phys. Rev. Lett. **100**, 148304 (2008).
[46] P. Tierno, Depinning and collective dynamics of magnetically driven colloidal monolayers, Phys. Rev. Lett. **109**, 198304 (2012).
[47] O. V. Dobrovolskiy, E. Begun, M. Huth, and V. A. Shklovskij, Electrical transport and pinning properties of Nb thin films patterned with focused ion beam-milled washboard nanostructures, New J. Phys. **14**, 113027 (2012).
[48] P. Martinoli, Static and dynamic interaction of superconducting vortices with a periodic pinning potential, Phys. Rev. B **17**, 1175 (1978).
[49] Q. Le Thien, D. McDermott, C. J. Olson Reichhardt, and C. Reichhardt, Orientational ordering, buckling, and dynamic transitions for vortices interacting with a periodic quasi-one-dimensional substrate, Phys. Rev. B **93**, 014504 (2016).
[50] D. McDermott, C. J. Olson Reichhardt, and C. Reichhardt, Stripe systems with competing interactions on quasi-one dimensional periodic substrates, Soft Matter **10**, 6332 (2014).
[51] C. Reichhardt, C. J. O. Reichhardt, I. Martin, and A. R. Bishop, Dynamical ordering of driven stripe phases in quenched disorder, Phys. Rev. Lett. **90**, 026401 (2003).
[52] C. Reichhardt and C. J. Olson Reichhardt, Depinning and nonequilibrium dynamic phases of particle assemblies driven over random and ordered substrates: a review, Rep. Prog. Phys. **80**, 026501 (2017).
[53] See Supplemental Material at http://link.aps.org/supplemental/10.1103/PhysRevResearch.6.023116 for supplemental videos.
[54] S. Shapiro, Josephson currents in superconducting tunneling: The effect of microwaves and other observations, Phys. Rev. Lett. **11**, 80 (1963).
[55] P. Martinoli, O. Daldini, C. Leemann, and E. Stocker, ac quantum interference in superconducting films with periodically modulated thickness, Solid State Commun. **17**, 205 (1975).
[56] L. Van Look, E. Rosseel, M. J. Van Bael, K. Temst, V. V. Moshchalkov, and Y. Bruynseraede, Shapiro steps in a superconducting film with an antidot lattice, Phys. Rev. B **60**, R6998 (1999).
[57] C. Reichhardt, R. T. Scalettar, G. T. Zimányi, and N. Grønbech-Jensen, Phase-locking of vortex lattices interacting with periodic pinning, Phys. Rev. B **61**, R11914 (2000).

[58] R. E. Thorne, J. S. Hubacek, W. G. Lyons, J. W. Lyding, and J. R. Tucker, ac-dc interference, complete mode locking, and origin of coherent oscillations in sliding charge-density-wave systems, Phys. Rev. B **37**, 10055 (1988).

[59] C. Reichhardt and C. J. O. Reichhardt, Shapiro steps for skyrmion motion on a washboard potential with longitudinal and transverse ac drives, Phys. Rev. B **92**, 224432 (2015).